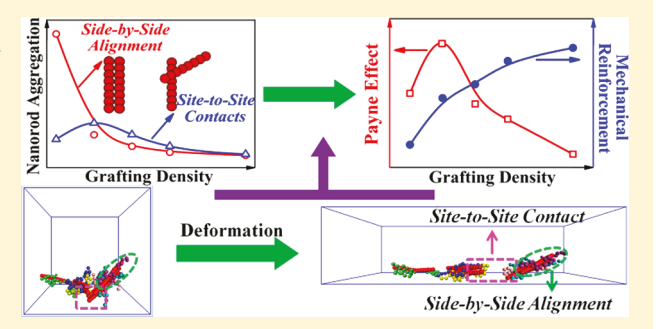
## 

### Mechanical and Viscoelastic Properties of Polymer-Grafted Nanorod Composites from Molecular Dynamics Simulation

Jianxiang Shen,\*,†® Xue Li,‡ Liqun Zhang,<sup>§®</sup> Xiangsong Lin,† Haidong Li,† Xiaojun Shen,† Venkat Ganesan,\*,<sup>|®®</sup> and Jun Liu\*,<sup>§®</sup>

Supporting Information

ABSTRACT: An understanding of the structure-property relationship in polymer/nanorod (NR) nanocomposites is of fundamental importance in designing and fabricating polymer nanocomposites (PNCs) with desired properties. Here, we study the structural, mechanical, and viscoelastic properties of polymergrafted NR filled PNCs, using coarse-grained molecular dynamics simulation. The mechanical reinforcement efficiency is found to be determined by the NR/polymer interfacial properties, which are in turn modulated by the grafting density, the grafted chain length, and the graft-matrix interaction strength. By systematically analyzing the evolution of the polymer-grafted NRs during



mechanical deformation, we find that the NRs aligning side by side with each other do not contribute much to the mechanical reinforcement. Simulation results also indicate that the strain-dependent viscoelastic behavior (the Payne effect) originates from the failure of the local filler network and, especially, NR clusters constructed via site-to-site contacts. PNCs with low grafting density and short grafted chains are found to form NR aggregates, mostly through the site-to-site contact state, which leads to a more pronounced Payne effect as reflected in the slope of the storage modulus versus shear amplitude. Furthermore, for stronger graft-matrix interactions, the NRs dispersed in the polymer matrix act as the temporary cross-linking points for a polymer shell layer-bridged NR network, accounting for the significant improvement in the mechanical property and the large increase in the Payne effect at high graft-matrix interaction strengths. In general, higher grafting density, longer grafted chains, and moderate graft-matrix interactions can effectively minimize the nonlinear viscoelastic behavior of PNCs.

#### 1. INTRODUCTION

Polymer nanocomposites (PNCs) composed of one-dimensional nanorods (NRs) have attracted considerable interest, and many potential applications have been proposed such as optical devices, 1,2 biosensing, 3 semiconducting devices, 4 photovoltaic devices,<sup>5</sup> etc. However, two significant challenges still confront the realization of the full potential of NR-based PNCs: controlling the microstructure and morphology of the NRs and developing a predictive understanding of morphologyproperty relationships.6

The most widely used strategy to regulate the spatial organization of the NRs in the polymer matrix is to graft polymer chains onto the NRs to form polymer layers. By tuning the graft-matrix interfacial interactions, polymer-grafted NRs in PNCs have been shown to form a variety of different equilibrated structures, such as end-to-end alignment, side-byside alignment, isolated NRs, and other irregular structures.<sup>7–10</sup> Considerable theoretical and experimental efforts have been devoted to understanding the dispersion behavior of polymergrafted NRs influenced by various factors such as the grafting density, the grafted chain length, the aspect ratio of NRs, the NR volume fraction, etc. 11-17 For example, uniformly grafted NRs were found to be preferentially aligned side-by-side to form the thermodynamic stable aggregation state. 10 By increasing the NR volume fraction, the NR arrangements gradually evolve from the well-dispersed state to the side-byside alignment, to the end-to-end alignment, and to a percolated network formed by end-to-end alignment.<sup>18</sup> Our previous work also indicated that the polymer-grafted NRs evolved from a macroscopic phase-separated state between NRs and polymer matrix, to a homogeneous dispersion of NRs, and to "tele-bridging" of NRs via matrix chains by increasing the miscibility between grafted chains and matrix chains. 19

Received: January 25, 2018 Revised: March 15, 2018 Published: March 28, 2018

<sup>&</sup>lt;sup>†</sup>Department of Polymer Science and Engineering, Jiaxing University, Jiaxing 314001, P. R. China

<sup>&</sup>lt;sup>‡</sup>Department of Chemical and Textile Engineering, Jiaxing University Nanhu College, Jiaxing 314001, P. R. China

<sup>§</sup>Key Laboratory of Beijing City on Preparation and Processing of Novel Polymer Materials, Beijing University of Chemical Technology, Beijing 100029, P. R. China

Department of Chemical Engineering, The University of Texas at Austin, Austin, Texas 78712, United States

Understanding the factors controlling the mechanical and viscoelastic properties of nanocomposites is of crucial importance in tailoring the processing and manufacturing properties. However, while numerous fundamental studies have been conducted to understand how various factors influence the dispersion behavior of NRs, the effect of grafted polymer chains on the resulting mechanical and viscoelastic properties of PNCs has received considerably less attention. 1,20-22 instance, by preparing the polyurethane nanocomposites composed of ZnO NRs, Kroener et al. found that the tensile modulus was improved by surface modification of NRs.<sup>23</sup> Similar results were obtained by Wang et al. using 4,4'diphenylmethane diisocyanate-grafted attapulgite NRs.<sup>2</sup> bon nanotubes (CNTs) grafted with polymer chains or small molecules have also proven to efficiently enhance the mechanical and thermal properties of CNT-based PNCs due to the improved interfacial interactions. 25,26 However, the dependence of the mechanical and viscoelastic properties of PNCs on the microstructure of polymer-grafted NRs remains

Computer simulation techniques provide an attractive approach to probe the structure-property relationships of PNCs. For example, the nucleation and growth of voids in PNCs containing bare NRs were directly probed by Toepperwein and de Pablo using coarse-grained Monte Carlo (MC) and molecular dynamics (MD) simulations.<sup>27</sup> They also investigated the influence of the aspect ratio of bare NRs on the mechanical properties and the relaxation dynamics during the uniaxial deformation.<sup>28</sup> Balazs and co-workers combined Cahn-Hilliard theory and Brownian dynamics (BD) to predict the structural evolution and the mechanical property of PNCs containing bare NRs and found that the reinforcement efficiency of NRs in doubly percolating system was significantly increased.<sup>29</sup> However, the focus of such simulation studies has been on the structural and mechanical properties of PNCs composed of bare NRs, and relatively fewer studies have addressed the viscoelastic properties of PNCs containing polymer-grafted NRs. With the use of MD simulations, Arya et al. found that the multiblock copolymer composed of "hard" and "soft" segments would form interconnected, rod-shaped, hard domains surrounded by soft matrix, leading to the increase in mechanical reinforcement.<sup>30</sup> In other work, Hattemer and Arya also elucidated the role of spherical nanoparticle (NP) grafts in the frequency-dependent viscoelastic properties of PNCs using equilibrium MD simulations.<sup>31</sup> Raos and coworkers have carried out coarse-grained dissipative particle dynamics (DPD) simulations of polymer materials filled with spherical NPs to examine the effect of filler dispersion state on the Payne effect of PNCs in terms of the amplitude dependence of the storage modulus. 32,33 In our previous work, we investigated the effects of the grafting density and grafted chain length on the structural, mechanical, and viscoelastic properties of polymer-grafted spherical NP composites.<sup>34</sup> Our results suggested that the increased mechanical and reduced nonlinear viscoelastic properties were correlated to the favorable graft-matrix interfacial interactions.

Much of the above-discussed past studies have been concerned with the properties of polymer-grafted, *spherical* NPs dispersed in polymer matrices.<sup>35–37</sup> In contrast, little clarity exists on the influence of particle anisotropy, such as arising in the context of grafted NRs, on the mechanical and viscoelastic properties. Motivated by such issues, in the present work, we use coarse-grained molecular dynamics (CGMD)

simulations to understand how polymer chains grafted onto anisotropic NRs affect the mechanical and viscoelastic properties of PNCs. We here employ the same simulation systems as in our previous work which studied the dispersion/aggregation behavior of NRs. We systematically investigate the effects of the grafting density and grafted chain length on the tensile stress—strain behavior and the amplitude dependence of the storage modulus.

For filler-reinforced PNCs, an important feature is the nonlinear mechanical behavior and the resulting Payne effect. When subjected to small deformations, the elastic modulus has been observed to drop significantly, and the resulting decrease (relative to the original modulus) is quantified as the Payne effect. The Payne effect is of fundamental importance in applications such as the rolling resistance and the durability of rubbers. Motivated by such considerations, in this work, we probe the role of the grafted polymer chains on the NR dispersion state and the NRs/polymer interface and examine the evolution of the polymer-grafted NRs during the deformation to derive insights into the morphological features underlying mechanical reinforcement and the Payne effect. In addition, considering that the grafted polymer may not be chemically identical to the matrix polymer in most real applications, we also investigate the effect of the miscibility between grafted chains and matrix chains by tuning the thermodynamic interaction parameter between them. From our results, we find that the NRs in side-by-side alignment do not contribute significantly to the mechanical reinforcement, and the failure of NR clusters formed via site-to-site contacts is responsible for the Payne effect. Given that the grafting of the polymer chains onto NRs adds an adjustable parameter for tailoring the properties of PNCs, our results could provide guidelines for the optimization and design of such PNCs for specific applications.

#### 2. MODEL AND SIMULATION METHODS

2.1. Model and Interactions. In our simulations, we consider nanorods (NRs) uniformly grafted with polymer chains embedded in an un-cross-linked homopolymer matrix. The polymer chains are modeled as fully flexible bead-spring chains,  $^{39}$  with the length  $L_{
m m}$  for the matrix chains and  $L_{
m g}$  for the grafted chains. Depending on the simulated system,  $L_{g}$  ranges from 4 to 12 beads, and  $L_{\rm m}$  is fixed at 30 beads. In most experimental cases, the grafted chains are always much shorter than the matrix chains. Therefore, it is reasonable and practical to consider the case of  $L_{\rm g}$  <  $L_{\rm m}$ . Although the matrix chains considered in our simulations are rather short, they already display the typical behavior of polymer chains. The grafted chains composed of 4 or 6 monomers, however, are not polymeric but do closely mimic the shorter oligomers which are often used in NR dispersions. Since the chain length in our simulation is much shorter than the critical entanglement length, 40-42 our study is representative of unentangled systems. The total number of polymer beads in the simulation is 7200. The adjacent beads in each polymer chain are connected via a stiff finite extensible nonlinear elastic (FENE) potential:

$$U_{\text{FENE}} = -0.5kR_0^2 \ln \left[ 1 - \left( \frac{r}{R_0} \right)^2 \right]$$
 (1)

where  $k = 30\varepsilon/\sigma^2$  and  $R_0 = 1.5\sigma$ , guaranteeing a certain stiffness of the bonds while avoiding high-frequency modes and chain

crossing. Since it is not our aim to study any specific polymer, we use the reduced LJ units where  $\sigma$  and  $\varepsilon$  are set to unity. Thus, all calculated quantities are dimensionless. Furthermore, all nonbonded interactions between polymer beads, including matrix—matrix, matrix—graft, and graft—graft, are described by the truncated and shifted Lennard-Jones (LJ) potential:

$$U_{pp}(r) = \begin{cases} 4\varepsilon_{pp} \left[ \left( \frac{\sigma}{r} \right)^{12} - \left( \frac{\sigma}{r} \right)^{6} \right] + C & r < 2.5\sigma \\ 0 & r \ge 2.5\sigma \end{cases}$$
 (2)

where the site-to-site interaction is cut off at the distance of  $2.5\sigma$  to include the attractive part and C is a constant to guarantee that the potential energy is continuous everywhere. The interaction strength  $\varepsilon_{\rm pp}$  is set to 1.0. The graft–matrix interaction strength  $\varepsilon_{\rm gm}$  is modulated to mimic the compatibility between grafted chains and matrix chains.

The rigid NR is also constructed through the bead–spring model. <sup>19,43</sup> The bonded interaction between two consecutive beads is represented by a stiff harmonic potential:

$$U_{\text{bond}} = k_{\text{r}} (r - r_0)^2 \tag{3}$$

where  $k_{\rm r}=1000\varepsilon/\sigma^2$  is the spring constant. The equilibrium bond distance  $r_0$  is set to  $2\sigma/3$ , thereby conferring a smooth surface to the NR. Each NR consists of 16 beads, rendering the NR an aspect ratio of 11 and a diameter of  $1\sigma$ . We note that if we take the length unit  $\sigma$  to be on the order of 1–4 nm, then our NRs would correspond to small diameter Au NRs or CdSe NRs or short SWCNTs. Meanwhile, the shape of the inclusions is enforced by the bending potential:

$$U_{\text{bend}} = k_{\theta} (\theta - \theta_0)^2 \tag{4}$$

where  $k_{\theta}$  is equal to  $200\varepsilon/\mathrm{rad}^2$  to ensure the rodlike character.  $\theta$  is the bending angle between triplets of NR beads, and  $\theta_0$  is equal to  $180^\circ$ . The NR will indeed retain its shape even under the deformation, as evidenced by the change in the bonded energy and bending energy shown in Figure S1 of the Supporting Information. The pairwise interactions between NRs,  $U_{\rm nn}$ , and between NRs and polymer,  $U_{\rm np}$ , are governed by the same LJ potential function in eq 2 with the cutoff distance equal to  $r_{\rm cutoff}=2.5\sigma$ . The interaction strength parameters  $\varepsilon_{\rm nn}$  and  $\varepsilon_{\rm np}$  are both set to 1.0 in a unified manner.

The grafted chains are uniformly attached to the surface of NRs using FENE springs (eq 1). The number of grafted chains per NR,  $N_{\rm g}$ , is determined from the grafting density ( $\Sigma$ ) according to  $N_g = \Sigma \times \pi D_n L_n$ , where  $D_n$  is the cross-section diameter of NR and  $L_n$  is the length of NR. Since there is a oneto-one correspondence between  $\Sigma$  and  $N_{\rm g}$ , we use the parameter  $N_{\rm g}$  to denote the grafting density. The grafting density in our simulation ranges from  $N_g = 4$  to  $N_g = 20$ , covering a broad regime of grafted layers spanning from the mushroom to the brush conformation. The ratio of the radius of NRs to the radius of gyration of grafted chains ranges from 0.35 to 0.61. Thus, our simulations correspond to PNCs containing monodisperse rodlike fillers which are grafted with polymer chains of bigger size than the filler's diameter. All of our simulation systems contain 50 NRs with the volume fraction equal to 4.9%. Detailed information about the model PNCs with different grafting densities and grafted chain lengths is listed in Table 1.

**2.2. Molecular Dynamics Simulations.** The simulations are started from a nonoverlapped configuration of all the matrix

Table 1. Parameters of Each Simulation System Examined

| system | Σ    | $N_{ m g}$ | $L_{\rm g}/L_{\rm m}$ | $n_{\rm g}/n_{\rm m}$ |
|--------|------|------------|-----------------------|-----------------------|
| 1      | bare | 0          | 0/30                  | 0/240                 |
| 2      | 0.12 | 4          | 6/30                  | 200/200               |
| 3      | 0.23 | 8          | 6/30                  | 400/160               |
| 4      | 0.34 | 12         | 6/30                  | 600/120               |
| 5      | 0.58 | 20         | 6/30                  | 1000/40               |
| 6      | 0.30 | 10         | 4/30                  | 500/173               |
| 7      | 0.30 | 10         | 8/30                  | 500/107               |
| 8      | 0.30 | 10         | 12/30                 | 500/40                |

<sup>a</sup>Surface grafting density =  $\Sigma$ , number of grafted chains per NR =  $N_{\rm gr}$  length of grafted chains =  $L_{\rm gr}$  length of matrix chains =  $L_{\rm mr}$  total number of grafted chains =  $n_{\rm gr}$  and total number of matrix chains =  $n_{\rm mr}$ .

chains and polymer-grafted NRs in a large simulation box. Then the NPT ensemble is applied to compress the simulation box by using the Nosé-Hoover thermostat and barostat, until the reduced number density of polymer is kept around  $\rho^*$  = 0.85, corresponding to the density of polymer melts.<sup>44</sup> During the simulation, periodic boundary conditions are implemented in all three directions to eliminate edge effects. The equations of motion are integrated using the velocity-Verlet algorithm with a time step  $\Delta t = 0.001\tau$ , where  $\tau$  denotes the LJ time unit  $\tau = (m\sigma^2/\varepsilon)^{1/2}$ . The obtained structures are further equilibrated under the NVT ensemble with  $T^* = 1.0$ , which is far above the glass transition temperature of PNC systems examined (see Figure S2 of the Supporting Information). The equilibration process is performed over a long time (more than 1 million timesteps for our simulation) to ensure that each polymer chain has moved at least  $2R_{\sigma}$  ( $R_{\sigma}$  is the radius of gyration of polymer chain). We collect the structure and dynamics data for ensemble average, and statistical error bars are included to indicate the standard deviation of data.

After sufficient equilibrium, the uniaxial deformation and the oscillatory shear deformation are applied via the SLLOD equations of motion.<sup>45</sup> During the uniaxial deformation, the simulation box is stretched to a strain of  $\varepsilon_{\mathrm{T}}$  in the tensile direction, while the box lengths in the other two directions are simultaneously adjusted to keep the volume constant. This is because rubbery materials are often regarded as incompressible during the deformation process.<sup>46</sup> The tensile strain rate  $\dot{\varepsilon}_{\rm T}$  is set to be  $0.0327/\tau$ , which is the same as the simulation work from Gao et al. 47,48 Independent tests confirmed that the qualitative features of the results presented herein are independent of the strain rate (Figure S3). The average tensile stress  $\sigma_{\rm T}$  is obtained from the deviatoric part of the stress tensor  $\sigma_{\rm T} = (1 + \mu)(-P_{\rm T} + P)$ , where  $\sum_i (P_{ii}/3)$  is the hydrostatic pressure and  $P_{\rm T}$  is the normal pressure component in the strain direction. The parameter  $\mu$  stands for Poisson's ratio, which is equal to 0.5 here. It is noted that all the simulation results have been averaged over three independent directions.

During the oscillatory shear deformation, the upper xy-plane of the simulation box is shifted in both directions along the x-axis. The shear strain is characterized by a sinusoidal function  $\gamma(t) = \gamma_0 \sin(2\pi vt)$ , where  $\gamma_0$  and v are the oscillatory shear strain amplitude and shear frequency, respectively. To maintain the stability of the temperature in the system, the shear frequency is set to a low value of  $v = 0.001\tau^{-1}$  to ensure that the heat generated by the oscillations is removed from the system timely. Arguably, the low-frequency response is of more significance in practical applications of PNCs than the high-frequency response.<sup>31</sup> The shear strain amplitude ranges from

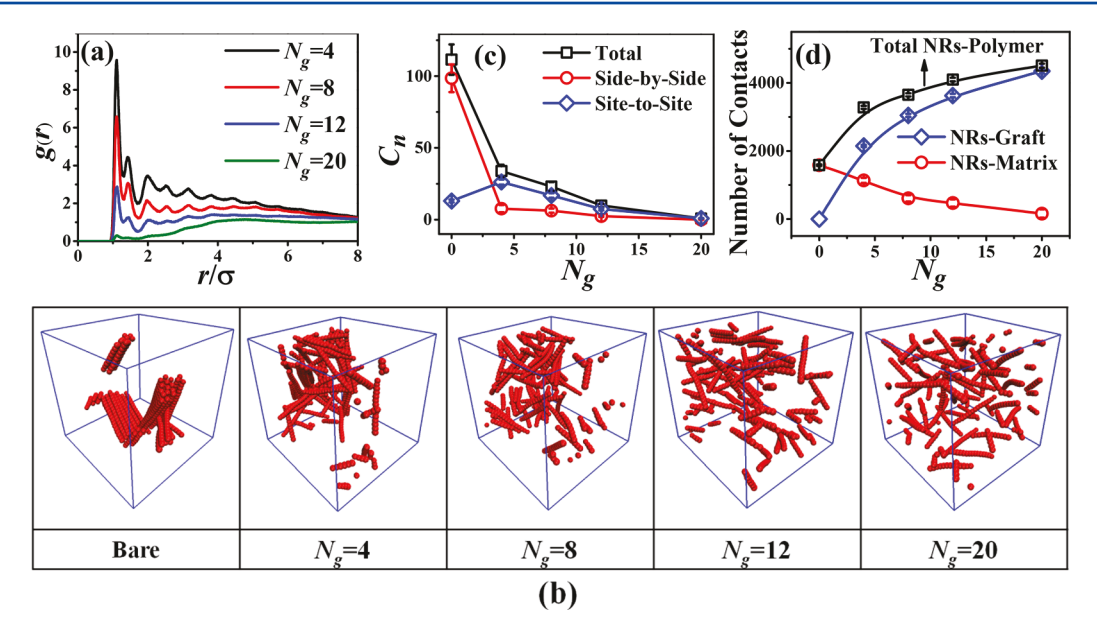


Figure 1. (a) Comparison of the inter-rod radial distribution functions g(r) for different grafting densities ( $N_g$ ). The grafted chain length is  $L_g = 6$ . (b) Snapshots of NR-filled polymer systems with different grafting densities. The red spheres denote the NR beads. For visual clarity, the polymer chains are not shown. (c) Ensemble averaged coordination number  $C_n$  as a function of grafting density. (d) Direct contacts of NRs with the matrix polymer segments, the grafted chain segments, and all the polymer segments as a function of grafting density.

0.05 to 0.5. The average shear stress  $\sigma_S$  is obtained from the deviatoric part of the stress tensor  $\sigma_S = P_{xz} = P_{zx}$ . For the oscillatory shear deformation, the shear stress can also be expressed by a sinusoidal function:

$$\sigma_{xy}(t) = \sigma_0 \sin(2\pi \nu t + \delta) = \sigma' \sin(2\pi \nu t) + \sigma'' \cos(2\pi \nu t)$$
(5)

where  $\sigma_0$  is the stress amplitude and  $\delta$  is the loss angle. Consequently, the storage modulus G' and the loss modulus G'' can be derived from the  $\sigma'$  and  $\sigma''$  parameters by  $G' = \sigma'/\gamma_0$  and  $G'' = \sigma''/\gamma_0$ . All the MD simulations are executed through the large scale atomic/molecular massively parallel simulator (LAMMPS) molecular dynamics package. More simulation details can be found in our previous work.

#### 3. RESULTS AND DISCUSSION

3.1. Effect of Grafting Density  $(N_{\alpha})$  on the Morphology. We begin by briefly discussing the influence of the grafting density  $N_{\rm g}$  on the morphology and structure of the NR composites. The graft-matrix interaction is set to  $\varepsilon_{\rm gm}$  = 1.0, modeling weak attraction between grafted chains and matrix chains. The inter-rod radial distribution functions (RDFs) corresponding to different grafting densities are shown in Figure 1a and the corresponding snapshots in Figure 1b. Bare NRs are seen to be agglomerated in a side-by-side manner (Figure 1b) with two distinct peaks in the radial distribution functions (Figure S4). With an increase in grafting density, the NRs are seen to become more dispersed, manifesting as a decrease in the intensity of the aggregation peaks. The side-byside assemblies of NRs disappear at the high grafting density of  $N_{\rm g}$  = 20, as shown in Figure 1b. Such results are in agreement with our previous work, <sup>19</sup> in which a more detailed analysis of the dispersion behavior and the underlying dispersion mechanisms were discussed.

In the transition of NR spatial distribution state from aggregation to uniform dispersion, the NRs in side-by-side alignment are seen to become reorganized into a combination

of (i) smaller clusters in side-by-side alignment, (ii) clusters formed via site-to-site contacts (such as end-to-end alignment, end-to-side alignment, etc.), and (iii) isolated NRs. In order to quantify such NR organization characteristics, we have calculated the ensemble averaged coordination number,  $C_n$ which is defined as the average number of neighboring NR beads within the center-to-center distance of  $1.25\sigma$  (connected by either site-to-site or side-by-side). The computation procedure of side-by-side alignment and site-to-site contact between NRs is described in detail in the Supporting Information. As seen in the results displayed in Figure 1c, bare NRs preferentially aggregate in a side-by-side manner, whereas for the polymer-grafted NRs, the majority of NR aggregations are in the site-to-site contact state. Further, the total coordination number of polymer-grafted NRs is seen to be dramatically reduced by raising the grafting density. Notably, the isolated NRs increase monotonically with the increase of the grafting density, suggesting the significant improvement in the NR dispersion. 19

In addition to the NR dispersion, the interfacial binding/ mixing between NRs and polymer chains is another critical factor governing the mechanical and viscoelastic properties of NRs filled PNCs. To characterize such properties, the number of direct contacts between NRs and polymer segments was quantified as a measure of the overall NRs/polymer interface, and the results are displayed in Figure 1d. Based on our simulation model, the NR is considered to directly contact with polymer segments when the center-to-center distance between any of NR beads and polymer bead is less than  $1.25\sigma$ , the first peak position in the radial distribution function. When the grafting density increases, the NRs will contact with more grafted chains and less matrix chains, with the net effect of increase in total NRs-polymer contacts. As expected, it is seen that the NR dispersion state is inextricably linked to the total NRs/polymer interface. Besides, we note that despite the decrease of the NRs-matrix contacts, the overall NRs-matrix interface is actually improved (as a consequence of being in the

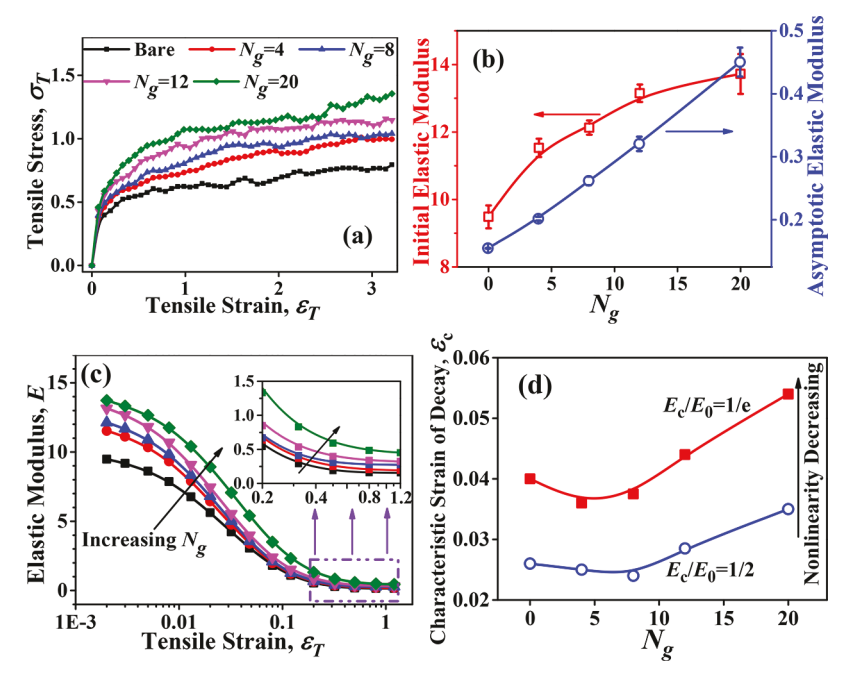


Figure 2. (a) Tensile stress—strain curves of simulated PNC systems with different grafting densities. (b) Initial elastic modulus and the asymptotic elastic modulus as a function of grafting density. (c) Elastic modulus—strain curves obtained from the fitted stress—strain curves through the equation of  $\sigma_{\rm T}/(\lambda-\lambda^{-2})=C_1+C_2/(C_3\lambda+C_4\lambda^{-2}+C_5)$ , where  $C_{i=1-5}$  is the fitting parameter and  $\lambda=1+\varepsilon_{\rm T}$ . (d) Characteristic strain of decay for the elastic modulus  $\varepsilon_{\rm c}$  plotted vs grafting density.

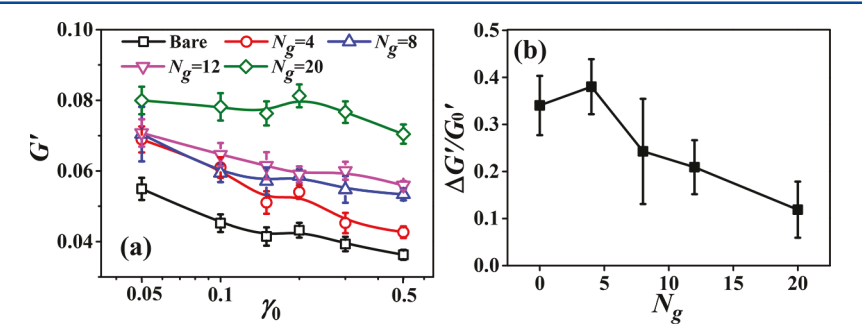


Figure 3. (a) Storage modulus versus dynamic strain amplitude for simulated systems with different grafting densities. The shear frequency is  $v = 0.001\tau^{-1}$ . (b) Storage modulus drop  $(\Delta G'/G'_0)$  as a function of grafting density. The grafted chain length is  $L_g = 6$ .

wet brush regime,  $N_{\rm g} \ge 8$ ), <sup>17,19</sup> as demonstrated by the increase in the matrix monomer density around the NRs (Figures S5 and S6). Such a behavior can be ascribed to the increase in the mixing entropy of the graft and matrix upon wetting.

3.2. Mechanical Properties and Dynamical Viscoelastic Response of PNCs. Having quantified the effect of the grafting density on the NR dispersion state and the NRs/polymer interface, we now discuss the results for mechanical properties of NR filled PNCs. Figure 2a displays the tensile stress—strain behavior for different grafting densities. As can be seen, each PNC exhibits an elastic response under very small deformation, followed by the strain softening at larger deformations. With an increase of the grafting density, the tensile stress under the same strain is markedly enhanced, indicating better mechanical reinforcement.

To better quantify the mechanical properties, the instantaneous elastic modulus, which is defined as the ratio of the tensile stress to the tensile strain, is obtained from the fitted stress—strain curves. The fitting equation is expressed as  $\sigma_{\rm T}/(\lambda-\lambda^{-2})=C_1+C_2/(C_3\lambda+C_4\lambda^{-2}+C_5)$ , where  $C_{i=1-5}$  is the fitting parameter and  $\lambda=1+\varepsilon_{\rm T}$ . A detailed description of the

curve fitting is given in the Supporting Information. In Figure 2c, the dependence of the elastic modulus on the tensile strain is plotted. It is seen that the elastic modulus is almost constant when the system is subjected to small deformations but drops sharply by nearly 2 orders of magnitude with further increase of the tensile strain and reaches an asymptotic value at relatively large strains. In particular, the initial elastic modulus, which gives the indication of the mechanical reinforcement, is seen to be improved by increasing the grafting density. Further, the asymptotic elastic modulus is also seen to increase with the grafting density.

Qualitatively, the strain-induced nonlinear behavior of the elastic modulus is quite similar to the experimentally observed "Payne effect", the features of which were discussed earlier. <sup>50</sup> In order to quantify the dependence of the nonlinear behavior on the grafting density, we have calculated the characteristic strain of the decay for the elastic modulus,  $\varepsilon_c$ , which is defined as the strain when the elastic modulus decays to a certain value (e.g.,  $E_c/E_0 = 1/e$  or  $E_c/E_0 = 1/2$ ). The characteristic strain typically measures the decay rate of the elastic modulus with respect to the tensile strain and can serve to quantify the nonlinear

behavior of PNCs. From the results displayed in Figure 2d, it can be seen that with an initial increase in the grafting density, the characteristic strain of the decay becomes slightly reduced. However, with further increase of the grafting density, the characteristic strain of the decay increases substantially, indicating a significant *reduction* in the nonlinear behavior of the PNCs.

In the context of *viscoelastic* properties of PNCs, we again concentrate on the so-called "Payne effect", namely the amplitude dependence of the storage modulus. Figure 3a shows the storage modulus as a function of the dynamic strain amplitude for simulated systems with varying grafting densities. Herein again, the storage modulus of each PNC system is seen to fall off nonlinearly with the increase of the strain amplitude, which is in similar to the experimental observations of the Payne effect. S1-53 Besides, the PNC systems with more dense brushes exhibit much higher storage modulus under the same strain amplitude, reflecting more effective mechanical reinforcement. For instance, the storage modulus at low strain amplitude  $G'_{\gamma_0=0.5}$  and the storage modulus at high strain amplitude  $G'_{\gamma_0=0.5}$  are both seen to be enhanced with the increase of the grafting density.

To explicitly quantify the Payne effect from the viscoelastic properties, we calculate the storage modulus drop with increasing the strain amplitude  $(\Delta G'/G'_0 = (G'_{\gamma_0=0.05} - G'_{\gamma_0=0.5})/G'_{\gamma_0=0.05})$ . For elastomeric polymer materials, a smaller storage modulus drop  $\Delta G'/G'_0$  indicates a weaker Payne effect and less energy dissipation during the dynamic shear deformation. As shown in Figure 3b, the Payne effect of NR-filled composite materials  $(\Delta G'/G'_0)$  is gradually reduced by increasing the grafting density, with the exception the of  $N_g=4$  system which has a maximum storage modulus drop. Indeed, the behavior of these nonlinear characteristics is seen to be very similar to the change of the elastic modulus with respect to the tensile strain discussed in the context of Figure 2d.

The linear behavior of the PNC composites and the mechanical reinforcements evident in Figure 2 are consistent with the general picture that the grafted chains enhance the dispersion and the contact between the matrix and NRs (Figure 1d) and thereby influence the mechanical strength of PNCs. The nonlinear behavior of PNCs, on the other hand, is often attributed to the failure of rigid NR aggregates. In such a picture, it is counterintuitive that the nonlinear behavior as reflected in Figures 2d and 3b for bare NRs is a little weaker than that of PNCs with small grafting densities (e.g.,  $N_{\rm g}=4$  and  $N_{\rm g}=8$ ), despite the existence of more NR aggregates in the bare system. For a resolution of this apparent paradox and for clarification of the mechanisms underlying the nonlinear mechanical behavior, the evolution of the NR clusters during the uniaxial deformation will be discussed in section 3.3.

# **3.3.** Morphology of NR Clusters during Deformation. To understand the origin of the nonlinear mechanical behavior of the PNCs, we present results for the evolution of polymergrafted NR clusters during the uniaxial deformation. As a first step toward this objective, the snapshots of NR clusters at different tensile strains are shown in Figure 4. In the interest of clarity, only six typical NRs are shown. In quiescent conditions, the NR cluster is seen to be composed of two NRs in side-byside alignment, three NRs in side-by-side alignment, and a single NR, with each part connected by site-to-site contacts. As expected, the connections via site-to-site contact are continuously broken down during the deformation, while the side-by-

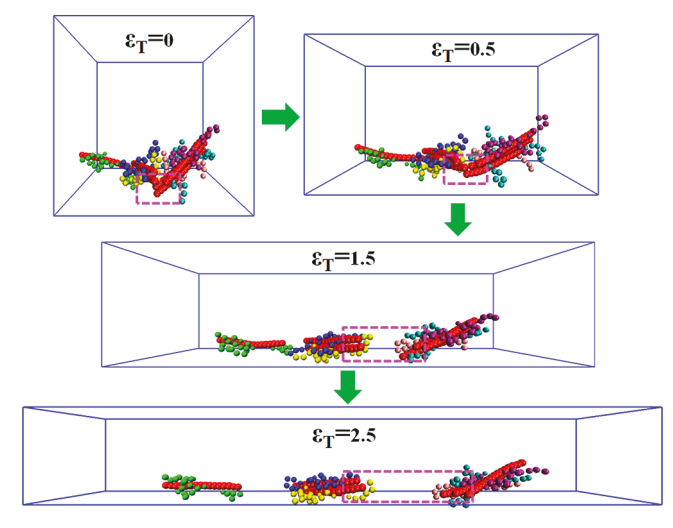


**Figure 4.** Microscopic deformation of the NR clusters during the tension process. For visual clarity, only six typical NRs are shown, and the matrix is not shown. The red spheres represent the rigid NRs, and the spheres with the other six colors denote the grafted chains attached to different NRs. Note that the size of polymer monomers is reduced to show the distribution of NRs within the simulation box. The grafting density is  $N_{\rm g}=4$ , and the grafted chain length is  $L_{\rm g}=6$ .

side alignment structure exhibits good stability. Especially, the complete rupture of the site-to-site contacts occurs at an estimated strain less than 0.5. Such observations hint that the breakdown of the site-to-site contacts are likely responsible for the reduction in the elastic modulus with increase in strain.

In order to probe the evolution of NR clusters during the tensile process, the changes in the total number of direct contacts between individual NRs were explicitly quantified. As is shown in Figure 5a, the contact number between NRs in side-by-side alignment almost remains unchanged as the tensile strain increases, with small fluctuations caused by perturbations of the parallel alignment. In contrast, the site-to-site contacts between NRs are seen to monotonically decrease during the tension process, exhibiting a correlation with the strain-dependent decline in the tensile elasticity (Figure 2c). This suggests that the linking points of NR clusters possibly act as stress concentration points, which when broken up early in the deformation account for the significant drop in the elastic modulus observed below the strain of 0.5.

While the disintegration of the NR clusters and the reduction in site-to-site contacts are seen to continue at larger strains (Figure 5a), a corresponding reduction in the elastic modulus is not however seen in the results in Figure 2c. We hypothesize that such results arise due to a combination of two factors: the NR orientation and the stress transfer between the grafted and matrix polymer chains. More explicitly, in Figure 5b we display the orientation of NRs as a function of the tensile strain. Here, the NR orientation is measured by the second Legendre polynomial, as given by  $\langle P_2 \rangle = \frac{1}{2}(3\langle \cos^2 \rangle - 1)$ , where  $\theta$ denotes the angle between the bond vector of NRs and the stretching direction. If  $\langle P_2 \rangle = 1$ , the NRs are perfectly aligned parallel to the stretching direction, while  $\langle P_2 \rangle = 0$  represents a completely random orientation of NRs. During the tension process, the polymer-grafted NRs are seen to become more oriented along the stretching direction. Interestingly, the rate of increase in the orientation of NRs via site-to-site contacts prevails over that of NRs in side-by-side. As a consequence of

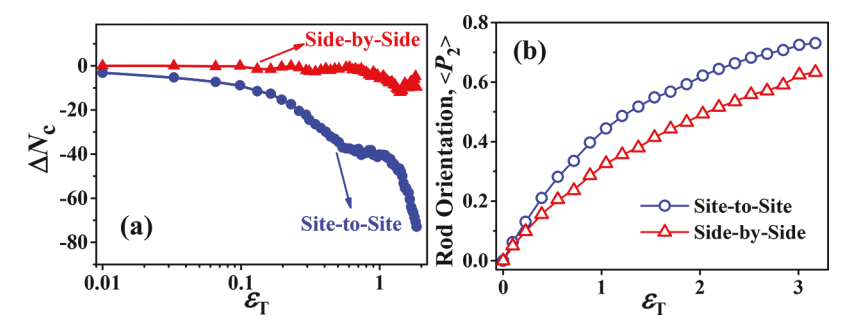


Figure 5. Comparison of NRs in side-by-side alignment and NRs via site-to-site contacts under uniaxial deformation: (a) changes of the total number of direct contacts between individual NRs; (b) rod orientation along the stretching direction. The grafting density is  $N_{\rm g}=4$ , and the grafted chain length is  $L_{\rm g}=6$ .

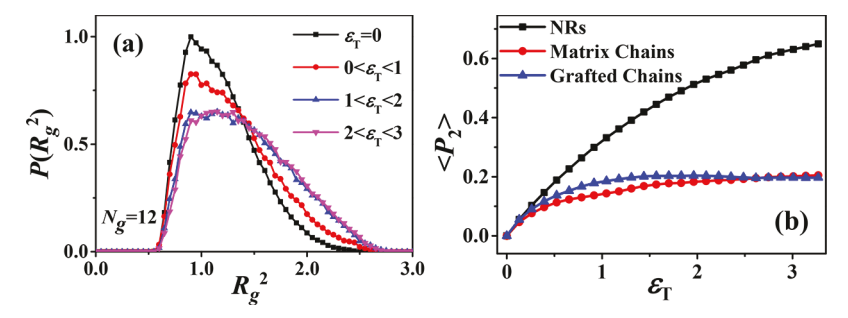


Figure 6. (a) Normalized distribution functions of the square radius of gyration of grafted polymer chains at different tensile strains. (b) Bond orientation of grafted chains and matrix chains along the stretching direction. For better comparison, the orientation of NRs is also added. The grafting density is  $N_g = 12$ , and the grafted chain length is  $L_g = 6$ .

such alignment in the direction of stretching, we expect that there will be a reduction in the contribution of such NR clusters to the elastic modulus.

A second (more speculative) factor also likely to reduce the impact of site-to-site clusters is the conformations of the grafted chains and its impact in stress transfer efficiency. To illustrate this, the conformations of the grafted chains during the uniaxial deformation were monitored. Figure 6a displays the normalized distribution functions of the square radius of gyration  $P(R_g^2)$  of grafted polymer chains at different tensile strains. The square radii of gyration is seen to exhibit a non-Gaussian distribution. During the tensile process, the grafted chains in the collapsed state  $(R_g^2 < 1.15$ , the  $\langle R_g^2 \rangle$  of free chains) and weakly stretched state (1.15  $< R_g^2 < 1.38$ ) are considerably reduced, with simultaneous increase in strongly stretched chains  $(R_g^2 > 1.38)$ . However, at strains larger than 1.0, further stretching of the grafted chains is seen to become restrained (such trends are also confirmed by the mean-square radius of gyration of grafted chains; see Figure S7).

Simultaneously, the bond orientations of grafted chains and matrix chains along the stretching direction were also probed (presented in Figure 6b). It is observed that the orientations of both the grafted and matrix chains increase for tensile strains less than 1.0 and reach a plateau for strains greater than 1.0. On the basis of the radius of gyration of the grafted chains and the orientational characteristics of the grafted and matrix chains, we speculate that at higher deformations there is likely to be slippage of polymer chains at the NRs/polymer interface that reduces the stress transfer. This second factor could also likely contribute to the mitigated influence of the tensile strain on the stress for larger deformations.

The above discussion, while speculative, provides a physical mechanism for the behavior of the elastic modulus discussed in the context of Figure 2. Explicitly, the results presented indicates that the linear values of the elastic modulus (Figure 2b) are seen to be principally determined by the NRs-polymer interface (Figure 1d) and are hence correlated to  $N_{\sigma}$ . In contrast, the nonlinear characteristics of the elastic modulus are seen to be correlated to the failure of rigid NR aggregates, the number of site-to-site contacts, and their evolution upon strain. Such a reasoning also rationalizes the nonintuitive behavior seen in Figure 2d, in which the nonlinear behavior for bare NRs was a little weaker than that of PNCs with small grafting densities (e.g.,  $N_g = 4$  and  $N_g = 8$ ), despite the existence of more NR aggregates in the bare system. Indeed, from Figure 1c, it is evident that the number of site-to-site contacts in the bare NR system is smaller than those of the grafted systems, and as a consequence the nonlinear behavior is also expected to be weaker.

We note that however the above mechanism underlying nonlinear behavior is not expected to persist for all grafting densities. Indeed, as noted in our previous research work,  $^{50}$  the nonlinear behavior of the  $N_{\rm g}=20$  system that contains minimal NR aggregation originates from the local NR network telebridged by the "rigid" polymer shell layer surrounding NRs. We will address the transition from the NR aggregate driven nonlinear behavior to the polymer network based nonlinear behavior in section 3.5.

**3.4. Effect of Grafted Chain Length** ( $L_{\rm g}$ ). Now, we extend our efforts to study the effect of the grafted chain length  $L_{\rm g}$  on the structural, mechanical, and viscoelastic properties of PNCs. The grafting density is fixed at  $N_{\rm g}=10$ , corresponding to a relatively dense brush, and the graft—matrix interaction is also set as  $\varepsilon_{\rm gm}=1.0$ . With the increase of the grafted chain length, the dispersion state of NRs is significantly improved, as indicated by the snapshots and the inter-rod radial distribution

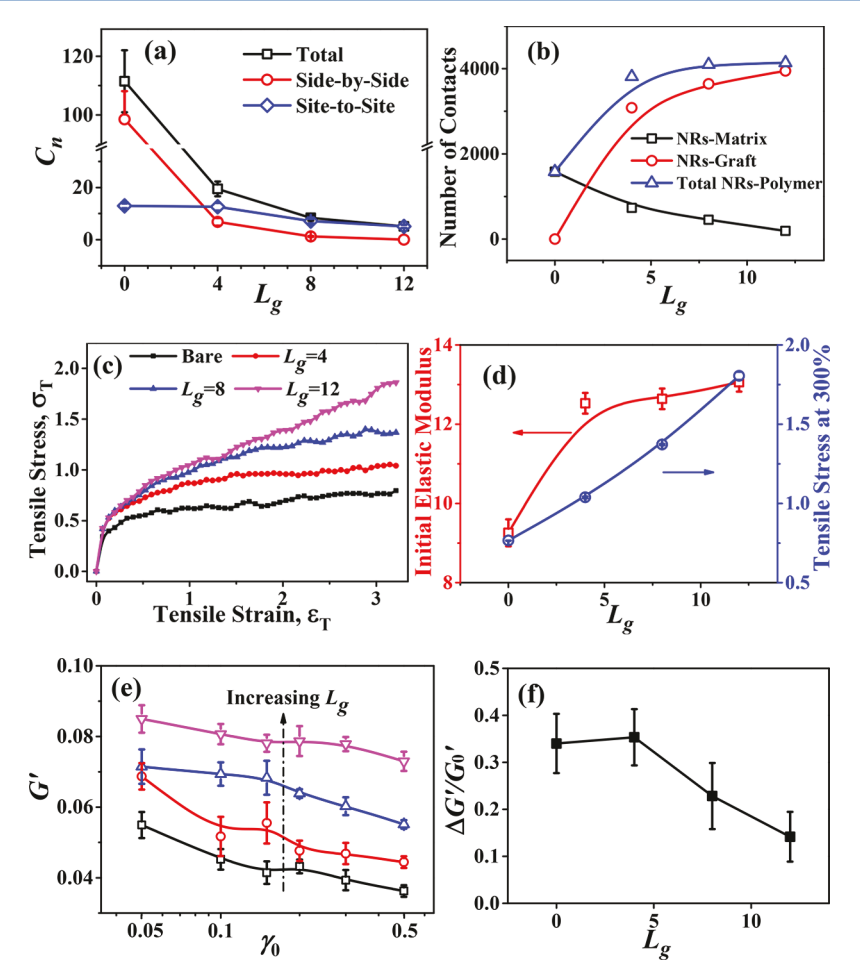


Figure 7. Influence of the grafted chain length on (a) the ensemble averaged coordination number  $C_{n'}$  (b) the direct contacts of NRs with polymer segments, (c) the tensile stress—strain curves of PNCs, (d) the initial elastic modulus (the left axis) and the tensile stress at 300% extension (the right axis), (e) the amplitude dependence of storage modulus, and (f) the storage modulus drop  $(\Delta G'/G'_0)$ . The grafting density is  $N_g = 10$ .

function (Figures S8 and S9). To be more specific, the NR clusters in side-by-side alignment are monotonically reduced by increasing the grafted chain length, while the NR clusters via site-to-site contacts still exist in large quantity in the  $L_{\rm g}=4$  system but tend to decrease with further increase of the grafted chain length, as suggested by the ensemble averaged coordination number in Figure 7a. The NRs/polymer interface was characterized by counting the number of direct contacts of NRs with polymer segments, as shown in Figure 7b. Similar to the trends seen with increasing the grafting density (Figure 1d), the NRs/polymer interface is seen to be greatly enhanced with increasing  $L_{\rm g}$ .

The tensile stress—strain curves of PNCs corresponding to different grafted chain lengths are compared in Figure 7c. It is seen that the tensile stress is considerably improved by increasing the grafted chain length. Additional information on the mechanical reinforcement can be obtained by further calculating the initial elastic modulus as a function of the grafted chain length, as shown in Figure 7d. With the increase of the grafted chain length, the initial elastic modulus is greatly increased, indicating the enhancement of the mechanical properties of PNCs. The increasing reinforcement effect can also be verified by the dynamic storage modulus in Figure 7e. The curves of storage modulus G' are shifted to larger G' along the grafted chain length, reflecting the better mechanical reinforcement. Both  $G'_{\gamma_0=0.05}$  and  $G'_{\gamma_0=0.5}$  are enhanced by

lengthening the grafted polymer chains (Figure 7f). These results are in agreement with the earlier discussion in which we correlated the linear elastic modulus of our model PNCs to the dispersion efficiency and the NR—polymer interfacial contacts (Figure 1).

To quantify the nonlinear behavior (Payne effect), the storage modulus drop  $\Delta G'/G'_0$  was calculated. As indicated by the decrease of  $\Delta G'/G'_0$  in Figure 7f, the Payne effect is weakened with longer grafted chains  $(L_g \ge 4)$ . Such results are again consistent with the mechanistic discussion presented in the preceding section and can be rationalized based on the siteto-site contacts between NRs (Figure 7a). Particularly, the  $L_{\sigma}$  = 12 system contains comparatively fewer site-to-site contacts and consequently exhibits a weaker Payne effect. It is worthwhile mentioning that the Payne effect of the  $L_g$  = 4 system is close to or maybe slightly higher than that of the bare system, although the two systems are approximately equal in the quantity of siteto-site contacts. Reasonably, the site-to-site contacts in the  $L_g$  = 4 system are somewhat reinforced by the grafted chains but are still destructible once subjected to loadings, leading to the slight enlargement of the Payne effect. Overall, our simulated results are consistent with the claim that the breakdown of local NR network via site-to-site contacts is responsible for the Payne effect in our PNC systems.

**3.5. Effect of Graft–Matrix Interaction (** $\varepsilon_{gm}$ **).** Considering that the grafted polymer may not in practice be chemically

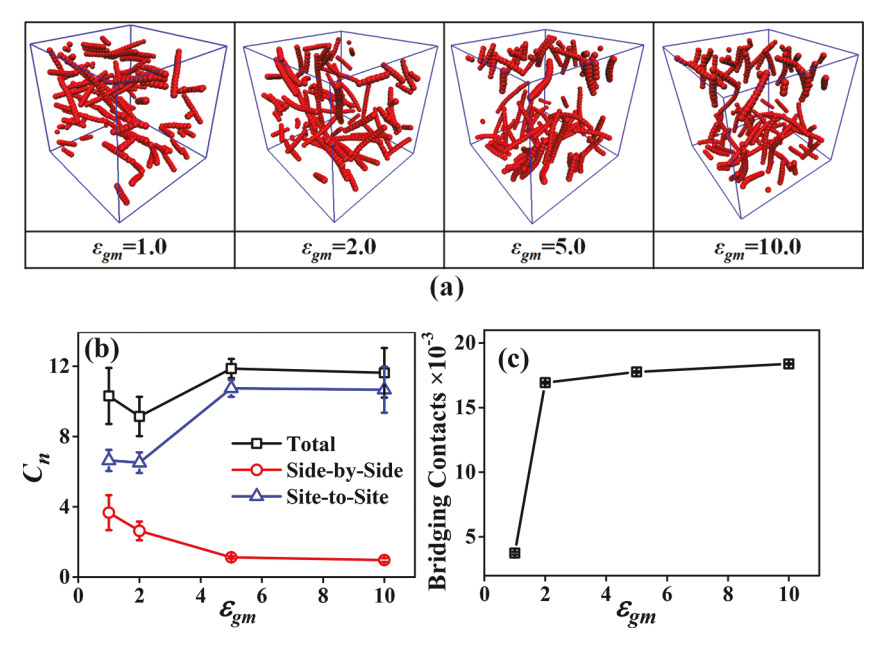


Figure 8. (a) Snapshots of PNC systems corresponding to different graft—matrix interactions ( $\varepsilon_{\rm gm}$ ). For visual clarity, the matrix are not shown. (b) Ensemble-averaged coordination number  $C_n$  plotted vs graft—matrix interaction. (c) Average bridging contacts of matrix chains with two grafted polymer layers or NRs. The grafting density is  $N_{\rm g} = 12$ , and the grafted chain length is  $L_{\rm g} = 6$ .

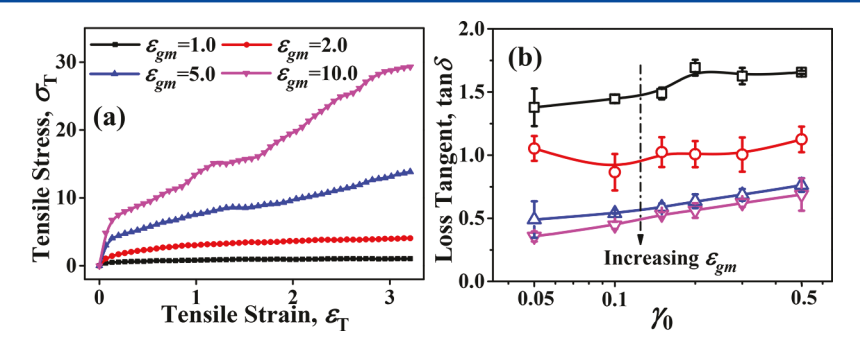


Figure 9. Influence of the graft—matrix interaction on (a) the tensile stress—strain curve and (b) the loss tangent (tan  $\delta$ ). The grafting density is  $N_g = 12$ , and the grafted chain length is  $L_g = 6$ .

identical to the matrix polymer, we now examine the influence of the miscibility between grafted chains and matrix chains by adjusting the interaction parameter between them ( $\varepsilon_{\rm gm}$ ). It should be noted that the NRs/polymer interfacial binding strength is significantly enhanced by the strong attraction between the grafted and matrix chains. In particular,  $\varepsilon_{\rm gm}=10.0$  roughly corresponds to the strength of hydrogen bonding when mapping the interaction parameter with the practical experimental system.

The snapshots in Figure 8a provide a visualization of the NR spatial distribution affected by the graft—matrix interaction. We find that the NRs become more dispersed by increasing the graft—matrix interaction from  $\varepsilon_{\rm gm}=1.0$  to  $\varepsilon_{\rm gm}=2.0$ , which can be ascribed to the enhanced wetting between the matrix chains and the grafted chains. However, as the graft—matrix interaction further increases ( $\varepsilon_{\rm gm}=5.0$  and 10.0), the dispersion state of NRs is seen to deteriorate to a small degree. Specifically, the NR clusters in side-by-side alignment are monotonically reduced with the increase of graft—matrix interaction, while the NR clusters via site-to-site contacts begin to increase at strong graft—matrix interaction. The interrod radial distribution function also signals that a good dispersion is obtained at intermediate graft—matrix interactions

(Figure S10). In addition, we find that the size of NRs/polymer interface described by the total direct contacts of NRs with polymer segments is also enhanced with the increase of graft—matrix interaction and then plateaus at strong graft—matrix interaction ( $\varepsilon_{\rm gm} > 2.0$ ). Specifically, the NRs—graft contacts are increased at high graft—matrix interactions, whereas the NRs—matrix contacts are reduced (Figure S11).

To explain the above-noted dispersion characteristics, we calculated the average number of polymer bridges between polymer-grafted NRs by counting the simultaneous contacts of matrix chains with two grafted polymer layers or NRs. In Figure 8c, the number of tele-bridging contacts is seen to increase significantly for stronger graft—matrix interactions ( $\varepsilon_{\rm gm} > 2.0$ ). Such bridging interactions are expected to serve as an attraction which brings the NRs closer and can be expected to contribute to a deterioration of the dispersion characteristics. <sup>19,54</sup>

Next, the effect of graft—matrix interaction on the mechanical behavior of PNCs will be studied. PNCs with stronger graft—matrix interaction are seen to exhibit better mechanical property, as indicated by the remarkable increase of the tensile stress under the same strain in Figure 9a. Interestingly, we observe two distinct characteristics from the stress—strain behavior. Explicitly, for  $\varepsilon_{\rm gm}$  < 2.0, the increase in the tensile

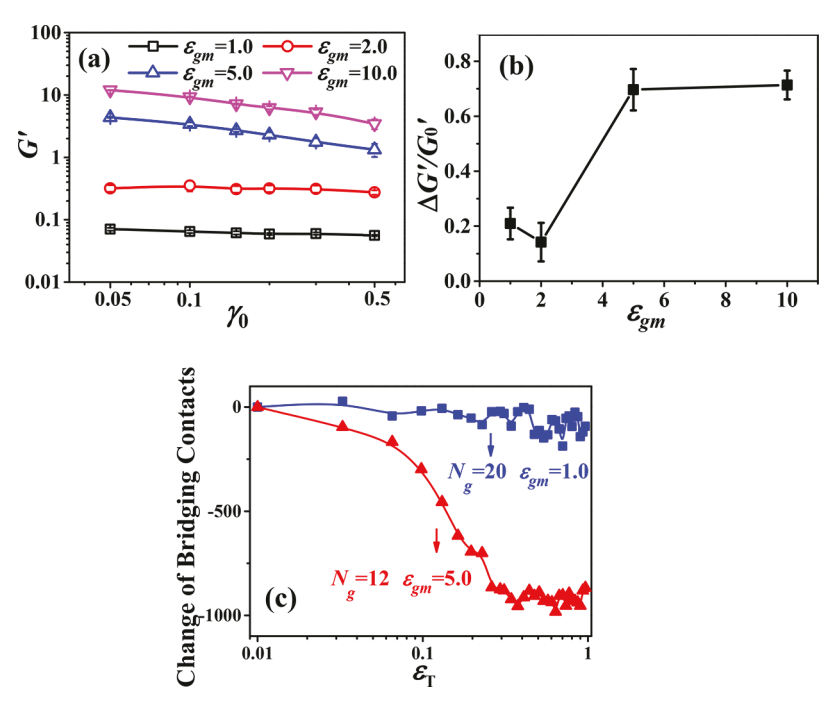


Figure 10. (a) Storage modulus of PNCs versus dynamic strain amplitude at different graft—matrix interactions. (b) Storage modulus drop ( $\Delta G'$ ) as a function of graft—matrix interaction. (c) Change of bridging contacts of matrix chains with two grafted layers or NRs during the uniaxial deformation.

stress is broadly correlated with the increase in the NR–polymer contacts (Figure S11a). Such a behavior is similar to those observed and discussed in the previous sections of this article. In contrast, for  $\varepsilon_{\rm gm} > 2.0$ , we do not observe a substantial enhancement in the NR–polymer contacts. Such a behavior suggests that a distinct mechanism is operative in underlying the mechanical properties for  $\varepsilon_{\rm gm} > 2.0$ .

To explain the above observation, especially with respect to the mechanical properties of  $\varepsilon_{\rm gm} > 2.0$ , we invoke the results presented in Figure 8c, which demonstrated the emergence of polymer-bridged particle structures for such regimes. On the basis of such an observation, we attribute the mechanical properties for such regimes to be an outcome of bridged NRs similar to a reversible three-dimensional polymer network with the NRs acting as the physical cross-linking points. Increasing  $\varepsilon_{\rm gm}$  is expected to slow down the segmental dynamics of the polymers in contact with the grafted layers and thereby strengthen such a network and the mechanical properties. <sup>55</sup>

To corroborate the above hypothesis on the role of polymer bridged network, we present results for the loss tangent  $(\tan \delta)$ , which is defined as the ratio of loss modulus to storage modulus  $((\tan \delta = G''/G'))$  and can be used as an indicator of the elastic effectiveness of the cross-linking network. The loss tangent will be much larger for the imperfect cross-linking network with low elasticity than for the nearly perfect one with high elasticity. Hence, the enhancement in physical cross-linking intensity can be indirectly demonstrated by the decline in the loss tangent with the increase of the graft—matrix interaction, as shown in Figure 9b.

The effect of graft—matrix interaction on the Payne effect was also examined. Figure 10a shows that the storage modulus is significantly improved with the increase of the graft—matrix interaction, revealing the enhancement in physical cross-linking intensity. Likewise, the Payne effect is evaluated by the storage modulus drop (Figure 10b). It is observed that PNCs with high graft—matrix interaction strength ( $\varepsilon_{\rm gm} \geq 5.0$ ) exhibit an

extraordinarily strong Payne effect. As noted above, the Payne effect for the PNCs with strong NRs/polymer interfacial interactions and thus NRs therein being separated from each other is likely ascribed to the breakdown of the local "rigid" polymer layer-bridged NR network. To illustrate this, we calculate the change of bridging contacts to indicate how the polymer layer-bridged NR network evolves during the deformation. From Figure 10c, for  $N_{\rm g}=20$  and  $\varepsilon_{\rm gm}=1.0$ , the change of the bridging contacts (with applied strain) is negligible. Such observations suggest that for low NRs/polymer interfacial strengths the bridging structures do not influence the Payne effect. Instead, as discussed in section 3.3 (which pertained to systems with  $\varepsilon_{\rm gm}=1.0$ ), the breakdown of the site-to-site clusters of NRs constitutes the main origin of Payne effect in such systems.

In contrast, the bridging contacts in PNC system with  $N_{\rm g}=12$  and  $\varepsilon_{\rm gm}=5.0$  are seen to decrease substantially under small deformations, demonstrating that the Payne effect at high graft—matrix interaction originates from the continuous breakdown of bridging structures. Interestingly, the PNCs with moderate graft—matrix interaction ( $\varepsilon_{\rm gm}=2.0$ ) has very few direct site-to-site contacts between NRs, and also the telebridging structures of NRs therein are still weak, exhibiting a considerably low Payne effect.

In sum, the above results demonstrate the (linear) mechanical properties of the PNC network to be determined to be two different physics depending on the strength of the interaction  $\varepsilon_{\rm gm}$ . For  $\varepsilon_{\rm gm} < 2.0$ , the NR–polymer interface serves as the main determinant of the mechanical reinforcement. For  $\varepsilon_{\rm gm} > 2.0$ , the polymer-bridged network plays a more influential role in determining the stress–strain response. The nonlinear strain response of the PNC confirms similarly distinct physics influencing the Payne effect.

#### 4. CONCLUSIONS

In this work, we comprehensively investigated the effect of the grafting density, grafted chain length, and the graft-matrix interaction on the mechanical and viscoelastic properties of PNCs composed of polymer-grafted NRs. Specifically, nonequilibrium coarse-grained molecular dynamics simulations were carried out to calculate the tensile stress-strain behavior and the amplitude-dependent storage modulus of PNCs. To better understand the underlying mechanism behind the mechanical reinforcement and the nonlinear dynamicalmechanical response (namely the "Payne effect"), we also systematically analyzed the evolution of the polymer-grafted NRs during the uniaxial deformation. For weak graft-matrix interactions, our results indicate that the mechanical reinforcement efficiency is primarily governed by the overall NRs/ polymer interface, which is inextricably linked to the NR dispersion state. The NRs/polymer interface would be enhanced by increasing the grafting density and grafted chain length, providing more mechanical reinforcement. Our results also indicate that the Payne effect originates from the failure of the local filler network and especially the evolution of the siteto-site contacts for NR-aggregation systems. For stronger graft-matrix interactions, the NRs being dispersed in polymer matrix act as the physical cross-linking points and meanwhile contribute to form the polymer shell layer-bridged NR network, accounting for the significant improvement in the mechanical property and the enhancement of the Payne effect at high graft-matrix interaction strength. Lastly, an interesting outcome of our work is the finding that increasing grafting density or grafted chain length, or keeping moderate graft-matrix interactions, can effectively reduce the nonlinear viscoelastic behavior of polymer-grafted nanorod composites. This work is expected to provide guidelines for designing and fabricating PNCs with enhanced mechanical and viscoelastic properties.

#### ASSOCIATED CONTENT

#### **S** Supporting Information

The Supporting Information is available free of charge on the ACS Publications website at DOI: 10.1021/acs.macromol.8b00183.

Part I: detailed analysis of the NR dispersion state and the NRs/polymer interface influenced by the grafting density, the grafted chain length, and the graft—graft interaction strength; part II: computation of side-by-side alignment and site-to-site contact between NRs; part III: curving fitting of the stress—strain relation calculated in the tensile test (PDF)

#### AUTHOR INFORMATION

#### **Corresponding Authors**

\*E-mail shenjx@mail.zjxu.edu.cn (J.S.).

\*E-mail liujun@mail.buct.edu.cn (J.L.).

\*E-mail venkat@che.utexas.edu (V.G.).

#### ORCID 6

Jianxiang Shen: 0000-0003-1991-8180 Liqun Zhang: 0000-0002-8106-4721 Venkat Ganesan: 0000-0003-3899-5843

#### **Notes**

The authors declare no competing financial interest.

#### ACKNOWLEDGMENTS

This work is supported by National Natural Science Foundation of China (51503081, 11502096), Natural Science Foundation of Zhejiang Province, China (LQ15B040002, Y16E030031), General Scientific Research Project of Department of Education of Zhejiang Province (Y201533251), and the Science and Technology Plan Projects of Jiaxing City, Zhejiang Province (2015AY11015). V.G. was partially supported by a grant from the Robert A. Welch Foundation (Grant F1599) and National Science Foundation (DMR1721512). Computations were performed at the Shanghai Supercomputer Center of China.

#### REFERENCES

- (1) Hore, M. J.; Composto, R. J. Functional polymer nanocomposites enhanced by nanorods. *Macromolecules* **2014**, *47*, 875–887.
- (2) Sharma, V.; Park, K.; Srinivasarao, M. Colloidal dispersion of gold nanorods: Historical background, optical properties, seed-mediated synthesis, shape separation and self-assembly. *Mater. Sci. Eng., R* **2009**, 65, 1–38.
- (3) Kabashin, A.; Evans, P.; Pastkovsky, S.; Hendren, W.; Wurtz, G.; Atkinson, R.; Pollard, R.; Podolskiy, V.; Zayats, A. Plasmonic nanorod metamaterials for biosensing. *Nat. Mater.* **2009**, *8*, 867–871.
- (4) Singh, A.; Gunning, R. D.; Sanyal, A.; Ryan, K. M. Directing semiconductor nanorod assembly into 1D or 2D supercrystals by altering the surface charge. *Chem. Commun.* **2010**, *46*, 7193–7195.
- (5) Talapin, D. V.; Nelson, J. H.; Shevchenko, E. V.; Aloni, S.; Sadtler, B.; Alivisatos, A. P. Seeded growth of highly luminescent CdSe/CdS nanoheterostructures with rod and tetrapod morphologies. *Nano Lett.* **2007**, *7*, 2951–2959.
- (6) Jancar, J.; Douglas, J.; Starr, F. W.; Kumar, S.; Cassagnau, P.; Lesser, A.; Sternstein, S. S.; Buehler, M. Current issues in research on structure-property relationships in polymer nanocomposites. *Polymer* **2010**, *51*, 3321–3343.
- (7) Thorkelsson, K.; Nelson, J. H.; Alivisatos, A. P.; Xu, T. End-to-End Alignment of Nanorods in Thin Films. *Nano Lett.* **2013**, *13*, 4908–4913.
- (8) Lee, A.; Andrade, G. F.; Ahmed, A.; Souza, M. L.; Coombs, N.; Tumarkin, E.; Liu, K.; Gordon, R.; Brolo, A. G.; Kumacheva, E. Probing dynamic generation of hot-spots in self-assembled chains of gold nanorods by surface-enhanced Raman scattering. *J. Am. Chem. Soc.* **2011**, *133*, 7563–7570.
- (9) Khani, S.; Jamali, S.; Boromand, A.; Hore, M. J.; Maia, J. Polymer-mediated nanorod self-assembly predicted by dissipative particle dynamics simulations. *Soft Matter* **2015**, *11*, 6881–6892.
- (10) Ting, C. L.; Composto, R. J.; Frischknecht, A. L. Orientational Control of Polymer Grafted Nanorods. *Macromolecules* **2016**, *49*, 1111–1119.
- (11) Hore, M. J.; Frischknecht, A. L.; Composto, R. J. Nanorod assemblies in polymer films and their dispersion-dependent optical properties. *ACS Macro Lett.* **2012**, *1*, 115–121.
- (12) Ferrier, R. C., Jr.; Koski, J.; Riggleman, R. A.; Composto, R. J. Engineering the Assembly of Gold Nanorods in Polymer Matrices. *Macromolecules* **2016**, *49*, 1002–1015.
- (13) Thorkelsson, K.; Bronstein, N.; Xu, T. Nanorod-based supramolecular nanocomposites: effects of nanorod length. *Macromolecules* **2016**, *49*, 6669–6677.
- (14) Kwon, T.; Ku, K. H.; Kang, D. J.; Lee, W. B.; Kim, B. J. Aspect-Ratio Effect of Nanorod Compatibilizers in Conducting Polymer Blends. *ACS Macro Lett.* **2014**, *3*, 398–404.
- (15) Park, J. H.; Joo, Y. L. Tailoring nanorod alignment in a polymer matrix by elongational flow under confinement: simulation, experiments, and surface enhanced Raman scattering application. *Soft Matter* **2014**, *10*, 3494–3505.
- (16) Rasin, B.; Chao, H.; Jiang, G.; Wang, D.; Riggleman, R. A.; Composto, R. J. Dispersion and alignment of nanorods in cylindrical block copolymer thin films. *Soft Matter* **2016**, *12*, 2177–2185.

(17) Frischknecht, A. L.; Hore, M. J. A.; Ford, J.; Composto, R. J. Dispersion of Polymer-Grafted Nanorods in Homopolymer Films: Theory and Experiment. *Macromolecules* **2013**, *46*, 2856–2869.

- (18) Jiang, G.; Hore, M. J.; Gam, S.; Composto, R. J. Gold nanorods dispersed in homopolymer films: optical properties controlled by self-assembly and percolation of nanorods. ACS Nano 2012, 6, 1578–1588
- (19) Shen, J.; Li, X.; Shen, X.; Liu, J. Insight into the Dispersion Mechanism of Polymer-Grafted Nanorods in Polymer Nanocomposites: A Molecular Dynamics Simulation Study. *Macromolecules* **2017**, 50, 687–699.
- (20) Hall, L. M.; Jayaraman, A.; Schweizer, K. S. Molecular theories of polymer nanocomposites. *Curr. Opin. Solid State Mater. Sci.* **2010**, *14*, 38–48.
- (21) Thorkelsson, K.; Bai, P.; Xu, T. Self-assembly and applications of anisotropic nanomaterials: A review. *Nano Today* **2015**, *10*, 48–66.
- (22) Chao, H.; Riggleman, R. A. Effect of particle size and grafting density on the mechanical properties of polymer nanocomposites. *Polymer* **2013**, *54*, 5222–5229.
- (23) Koerner, H.; Kelley, J.; George, J.; Drummy, L.; Mirau, P.; Bell, N. S.; Hsu, J. W.; Vaia, R. A. ZnO nanorod-thermoplastic polyurethane nanocomposites: morphology and shape memory performance. *Macromolecules* **2009**, *42*, 8933–8942.
- (24) Wang, C. H.; Shieh, Y. T.; Guo, G.; Nutt, S. Effects of organophilic-modified attapulgite nanorods on thermal and mechanical behavior of segmented polyurethane elastomers. *Polym. Compos.* **2010**, *31*, 1890–1898.
- (25) Yoon, J. T.; Lee, S. C.; Jeong, Y. G. Effects of grafted chain length on mechanical and electrical properties of nanocomposites containing polylactide-grafted carbon nanotubes. *Compos. Sci. Technol.* **2010**, 70, 776–782.
- (26) Khare, K. S.; Khabaz, F.; Khare, R. Effect of carbon nanotube functionalization on mechanical and thermal properties of cross-linked epoxy-carbon nanotube nanocomposites: role of strengthening the interfacial interactions. ACS Appl. Mater. Interfaces 2014, 6, 6098—6110.
- (27) Toepperwein, G. N.; de Pablo, J. J. Cavitation and crazing in rod-containing nanocomposites. *Macromolecules* **2011**, *44*, 5498–5509.
- (28) Toepperwein, G. N.; Riggleman, R. A.; de Pablo, J. J. Dynamics and Deformation Response of Rod-Containing Nanocomposites. *Macromolecules* **2012**, *45*, 543–554.
- (29) Buxton, G. A.; Balazs, A. C. Predicting the mechanical and electrical properties of nanocomposites formed from polymer blends and nanorods. *Mol. Simul.* **2004**, *30*, 249–257.
- (30) Arman, B.; Reddy, A. S.; Arya, G. Viscoelastic Properties and Shock Response of Coarse-Grained Models of Multiblock versus Diblock Copolymers: Insights into Dissipative Properties of Polyurea. *Macromolecules* **2012**, *45*, 3247–3255.
- (31) Hattemer, G. D.; Arya, G. Viscoelastic properties of polymer-grafted nanoparticle composites from molecular dynamics simulations. *Macromolecules* **2015**, *48*, 1240–1255.
- (32) Raos, G.; Moreno, M.; Elli, S. Computational Experiments on Filled Rubber Viscoelasticity: What Is the Role of Particle-Particle Interactions? *Macromolecules* **2006**, *39*, 6744–6751.
- (33) Raos, G.; Casalegno, M. Nonequilibrium simulations of filled polymer networks: Searching for the origins of reinforcement and nonlinearity. *J. Chem. Phys.* **2011**, *134*, 054902.
- (34) Shen, J.; Liu, J.; Li, H.; Gao, Y.; Li, X.; Wu, Y.; Zhang, L. Molecular dynamics simulations of the structural, mechanical and visco-elastic properties of polymer nanocomposites filled with grafted nanoparticles. *Phys. Chem. Chem. Phys.* **2015**, *17*, 7196–7207.
- (35) Ganesan, V.; Jayaraman, A. Theory and simulation studies of effective interactions, phase behavior and morphology in polymer nanocomposites. *Soft Matter* **2014**, *10*, 13–38.
- (36) Kumar, S. K.; Jouault, N.; Benicewicz, B.; Neely, T. Nanocomposites with Polymer Grafted Nanoparticles. *Macromolecules* **2013**, *46*, 3199–3214.

- (37) Allegra, G.; Raos, G.; Vacatello, M. Theories and simulations of polymer-based nanocomposites: From chain statistics to reinforcement. *Prog. Polym. Sci.* **2008**, *33*, 683–731.
- (38) Kumar, S. K.; Benicewicz, B. C.; Vaia, R. A.; Winey, K. I. 50th Anniversary Perspective: Are Polymer Nanocomposites Practical for Applications? *Macromolecules* **2017**, *50*, 714–731.
- (39) Kremer, K.; Grest, G. S. Dynamics of entangled linear polymer melts: A molecular-dynamics simulation. *J. Chem. Phys.* **1990**, *92*, 5057–5086.
- (40) Sethuraman, V.; Kipp, D.; Ganesan, V. Entanglements in Lamellar Phases of Diblock Copolymers. *Macromolecules* **2015**, 48, 6321–6328.
- (41) Karatrantos, A.; Clarke, N.; Composto, R. J.; Winey, K. I. Topological entanglement length in polymer melts and nanocomposites by a DPD polymer model. *Soft Matter* **2013**, *9*, 3877–3884
- (42) Qin, J.; Milner, S. T. Tubes, Topology, and Polymer Entanglement. *Macromolecules* **2014**, *47*, 6077–6085.
- (43) Toepperwein, G. N.; Karayiannis, N. C.; Riggleman, R. A.; Kröger, M.; de Pablo, J. J. Influence of nanorod inclusions on structure and primitive path network of polymer nanocomposites at equilibrium and under deformation. *Macromolecules* **2011**, *44*, 1034–1045.
- (44) Allen, M. P.; Tildesley, D. J. Computer Simulation of Liquids; Oxford University Press: 1989.
- (45) Evans, D. J.; Morriss, G. P. Statistical Mechanics of Nonequilbrium Liquids, 2nd ed.; Cambridge University Press: Cambridge, UK, 2008.
- (46) Rubinstein, M.; Colby, R. H. *Polymer Physics*; Oxford University Press: New York, 2003; Vol. 23.
- (47) Gao, J.; Weiner, J. Anisotropy effects on chain-chain interactions in stretched rubber. *Macromolecules* **1991**, *24*, 1519–1525.
- (48) Gao, J.; Weiner, J. Simulated polymer melt stress relaxation. I. Plateau behavior. *J. Chem. Phys.* **1995**, *103*, 1614–1620.
- (49) Plimpton, S. Fast parallel algorithms for short-range molecular dynamics. *J. Comput. Phys.* **1995**, *117*, 1–19.
- (50) Shen, J.; Liu, J.; Gao, Y.; Li, X.; Zhang, L. Elucidating and tuning the strain-induced non-linear behavior of polymer nanocomposites: a detailed molecular dynamics simulation study. *Soft Matter* **2014**, *10*, 5099–5113.
- (51) Cassagnau, P. Linear viscoelasticity and dynamics of suspensions and molten polymers filled with nanoparticles of different aspect ratios. *Polymer* **2013**, *54*, 4762–4775.
- (52) Rooj, S.; Das, A.; Heinrich, G. Tube-like natural halloysite/fluoroelastomer nanocomposites with simultaneous enhanced mechanical, dynamic mechanical and thermal properties. *Eur. Polym. J.* **2011**, 47, 1746–1755.
- (53) Agnelli, S.; Pandini, S.; Serafini, A.; Musto, S.; Galimberti, M. Anisotropic Nonlinear Mechanical Behavior in Carbon Nanotubes/Poly(1,4-cis-isoprene) Nanocomposites. *Macromolecules* **2016**, 49, 8686–8696.
- (54) Matsen, M. W.; Gardiner, J. Autophobic dewetting of homopolymer on a brush and entropic attraction between opposing brushes in a homopolymer matrix. *J. Chem. Phys.* **2001**, *115*, 2794–2804
- (55) Tauban, M.; Delannoy, J.-Y.; Sotta, P.; Long, D. R. Effect of Filler Morphology and Distribution State on the Linear and Nonlinear Mechanical Behavior of Nanofilled Elastomers. *Macromolecules* **2017**, *50*, *6369*–*6384*.